Supporting Information

Integration of Photovoltaic and Photogating Effects in WSe_2/WS_2/p-Si Dual Junction Photodetector Featuring High-Sensitivity and Fast-Response

Zihao Huang[1, 2], Yuchen Zhou[2, 3], Zhongtong Luo[2], Yibing Yang[2], Mengmeng Yang[4], Wei Gao[4], Jiandong Yao[1], Yu Zhao[2], Yuhua Yang[1], Zhaoqiang Zheng[2*] and Jingbo Li[4,5]*

[1] State Key Laboratory of Optoelectronic Materials and Technologies, Nanotechnology Research Center, School of Materials Science & Engineering, Sun Yat-sen University, Guangzhou 510275, Guangdong, P. R. China.

[2] Guangdong Provincial Key Laboratory of Information Photonics Technology, School of Materials and Energy, Guangdong University of Technology, Guangzhou 510006, Guangdong, P. R. China.

[3] Honor Device Co.,Ltd, Shenzhen 518000, Guangdong, P. R. China.

[4] Institute of Semiconductors, South China Normal University, Foshan 528225, Guangdong, P. R. China.

[5] Guangdong Provincial Key Laboratory of Chip and Integration Technology, Guangzhou 510631, P.R. China.

*Corresponding authors:

yangyuh3@mail.sysu.edu.cn and zhengzhq5@mail2.sysu.edu.cn

Supplementary Notes

Note S1: Calculation of surface potential difference (SPD):

The SPD between the AFM tip, WSe_2, WS_2 and p-Si can be calculated as follow:

$$eSPD_{WSe2} = \Phi_{WSe2} - \Phi_{tip} \quad (1)$$

$$eSPD_{WS2} = \Phi_{WS2} - \Phi_{tip} \quad (2)$$

$$eSPD_{p\text{-}Si} = \Phi_{p\text{-}Si} - \Phi_{tip} \quad (3)$$

where Φ_{WSe2}, Φ_{WS2}, $\Phi_{p\text{-}Si}$ and Φ_{tip} are the work functions WSe_2, WS_2, p-Si and the AFM tip, respectively.[1-2] Thus, the Fermi level difference (ΔE_{f1}) between WS_2 and WSe_2 can be obtained by

$$\Delta E_{f1} = \Phi_{WS2} - \Phi_{WSe2} = eSPD_{WS2} - eSPD_{WSe2} \quad (4)$$

Similarly, the Fermi level difference (ΔE_{f2}) between WS_2 and p-Si can be obtained by

$$\Delta E_{f2} = \Phi_{WS2} - \Phi_{Si} = eSPD_{WS2} - eSPD_{p\text{-}Si} \quad (5)$$

Note S2: Calculation of the key figures-of-merit for photodetectors

The important parameters that need to be calculated to better evaluate the optoelectronic performance of WSe_2/WS_2/p-Si device include responsivity (R), detectivity (D*), light on/off ratio (I_{on}/I_{off}), photoconductive gain (gain), and response time (τ_{rise} and τ_{decay}). The appeal parameters are computed by the following public statements: [3-5]

$$R = \frac{I_{ph}}{PS} = \frac{I_{light} - I_{dark}}{PS} \quad (6)$$

$$D^* = \frac{RS^{1/2}}{(2qI_{dark})^{1/2}} \quad (7)$$

$$I_{on} / I_{off} = \frac{I_{ph}}{I_{dark}} \quad (8)$$

$$\text{Gain}=\frac{\tau_t}{\tau_{transit}}=\left(\frac{I_p}{e}\right)\Big/\left(\frac{PS}{h\upsilon}\right)=hcR/(q\lambda) \tag{9}$$

where the electronic charge is defined as q, the effective sensing area is defined as S, the incident light density is defined as P, the Planck constant (6.626×10^{-34} J s^{-1}) is defined as h, light velocity is defined as c, the wavelength of the incident light is defined as λ, the photocurrent ($I_{ph} = I_{light} - I_{dark}$) is defined as I_{ph}, the device currents in light and darkness are I_{light} and I_{dark}, respectively.

Rise time ($\boldsymbol{\tau_{rise}}$) and decay time ($\boldsymbol{\tau_{decay}}$) are determined as the time elapsed between 10%/90% and 90%/10% of the pure photocurrent.[6]

Note S3: First-Principle Calculations

The theoretically results were based on the general gradient approximation (GGA) of Perdew, Burke and Ernzerhof (PBE), with the projector augmented plane-wave method in the Vienna Ab-initio Simulation Package (VASP) code.[7-11] The initial structure of three materials (monolayer WS_2, monolayer WSe_2 and bulk Si), set a vacuum larger than 15 Å around the slab for eliminating the interaction, built in Materials studio. All the atomic coordinates were fully relaxed with the force tolerance on 0.02 eV Å. The total energies calculation was set a plane-wave cutoff at 450 eV and a 15×15×1 Γ-center k-point grid. The electron density projection of the VBM (valence band maximum) and CBM (conduction band minimum) of the heterojunction material on the real space is calculated by the band decomposed charge densities method. The detailed calculation steps of this method can be obtained from the VASP manual.

Supplementary Figures

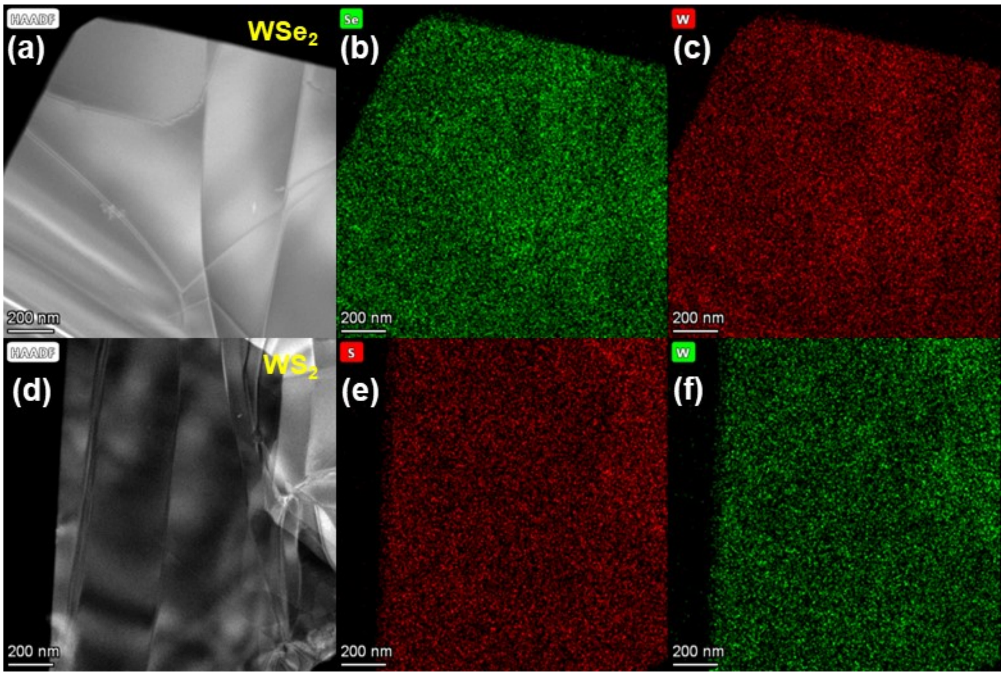

Figure S1. (a) Low-resolution TEM image of the WSe_2 flake. (b-c) Elemental distribution maps in the WSe_2 flake. (d) Low-resolution TEM image of the WS_2 flake. (e-f) Elemental distribution maps in the WS_2 flake.

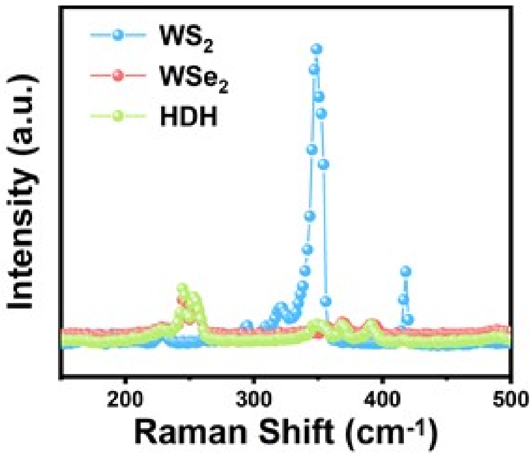

Figure S2. Raman spectra of the WSe_2, WS_2 and HDH heterostructures.

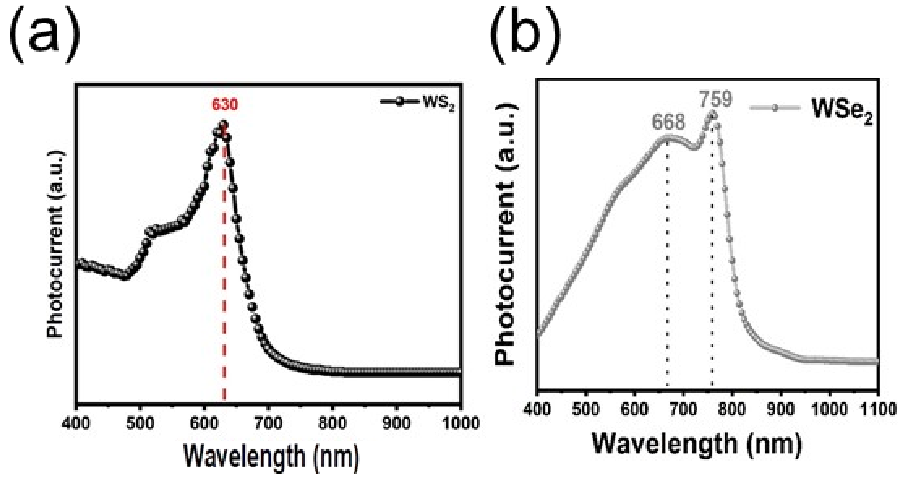

Figure S3. Spectral photocurrent of the (a) WS_2 and (b) WSe_2 devices at the range of 400−1100 nm. The WS_2 shows a photoresponse peak at 630 nm, and the WSe_2 shows two photoresponse peaks at 668 nm and 759 nm.

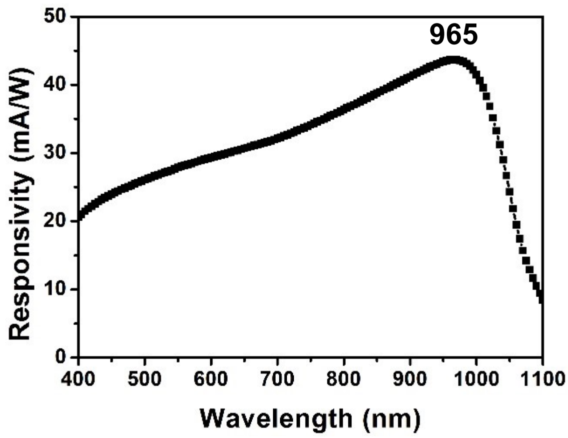

Figure S4. Spectral photocurrent of the commercial Si device (S120VC, Thorlabs) at the range of 400−1100 nm. The responsivity is less than 45 mA/W, and the photoresponse peak is 965 nm.

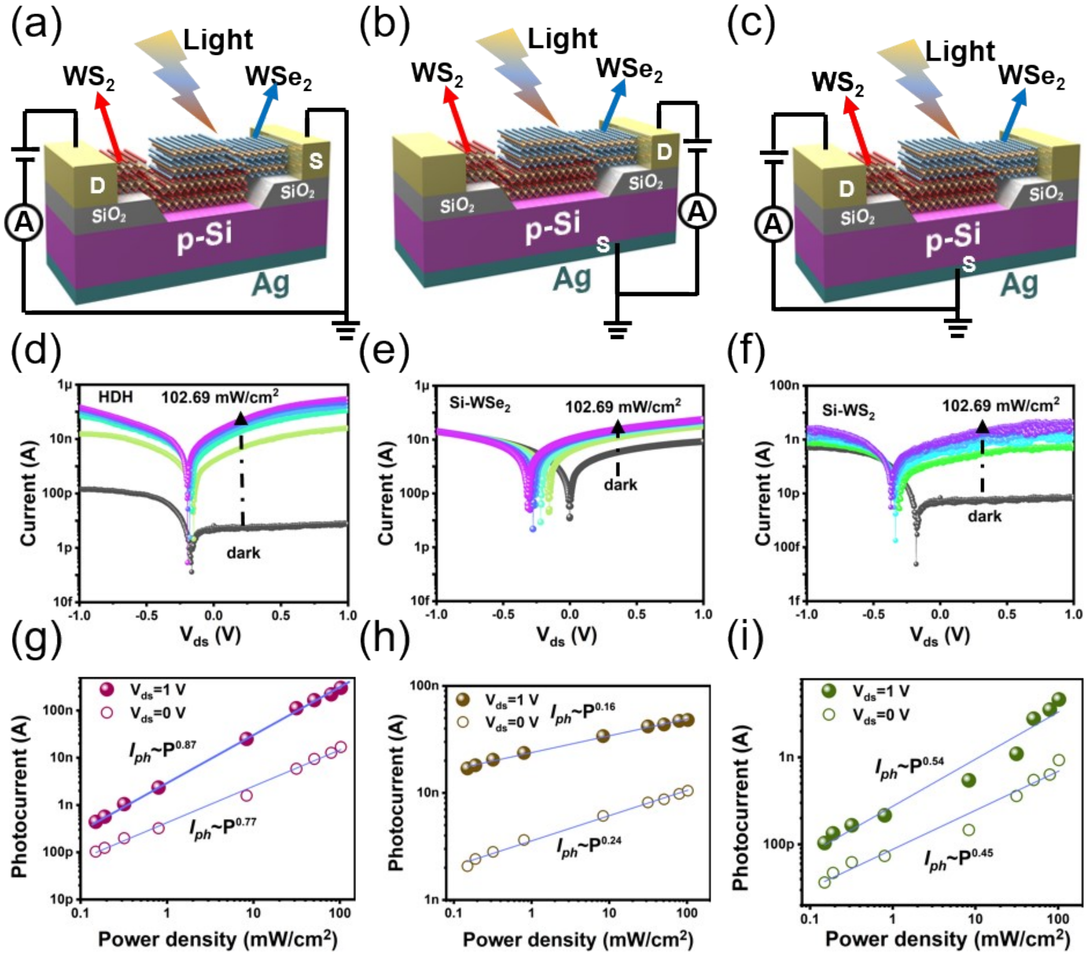

Figure S5. Structures and electrical connections of the constructed devices. (a) HDH device, where WS_2 is contacted with the drain and WSe_2 is contact with the source. (b) WSe_2/p-Si device, where WSe_2 is contact with the drain and p-Si is contact with the source. (c) WS_2/p-Si device, where WS_2 is contact with the drain and p-Si is contact with the source. *I*-*V* curves of the (d) HDH device, (e) WSe_2/p-Si device, and (f) WS_2/p-Si device under dark and illumination with various intensities. Photocurrent of the (g) HDH device, (h) WSe_2/p-Si device, and (i) WS_2/p-Si device as a function of illumination intensity at the bias of 0 V and 1 V.

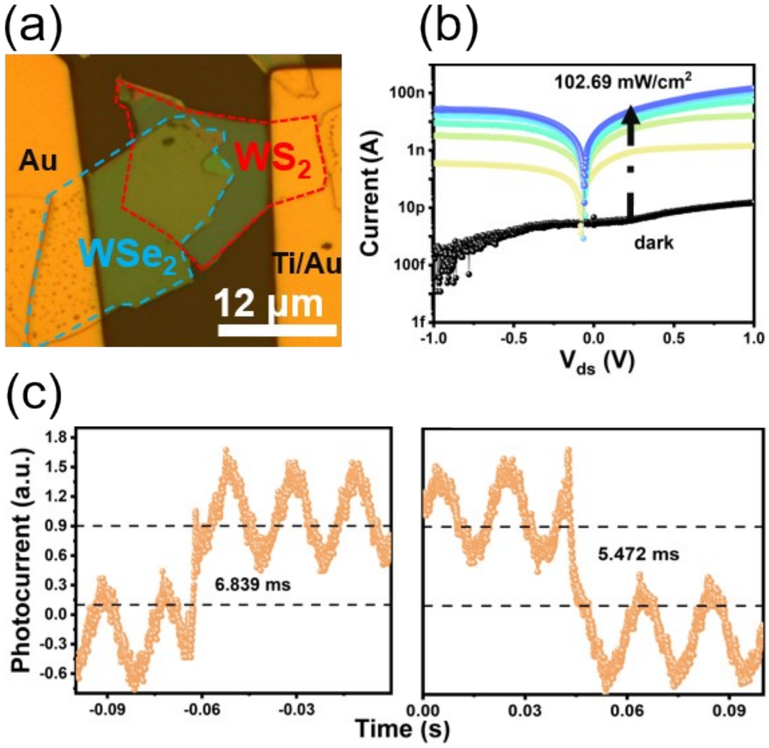

Figure S6. (a) Optical image of the WS_2-WSe_2 device. The WSe_2 and WS_2 flakes are marked in blue and red dashed lines, respectively. Source and drain are connected to the WSe_2 and WS_2, respectively. (b) *I-V* curves of the device in the dark and under 405 nm light irradiation with different powers. (c) Response time of the device at a voltage of -1 V. The corresponding τ_{rise} and τ_{decay} are 6.839 ms and 5.427 ms, respectively.

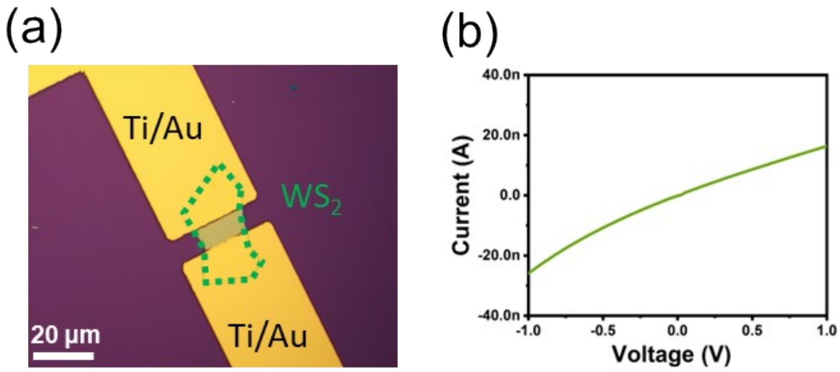

Figure S7. (a) Optical image of the WS_2 device. (b) *I-V* curve of the WS_2 device in the dark. The device shows linear *I-V* curve in the dark, indicating ohmic contact between the Ti/Au electrodes and WS_2.

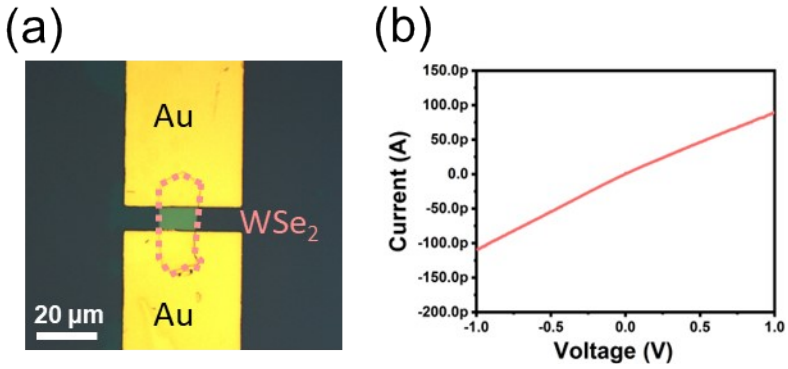

Figure S8. (a) Optical image of the WSe_2 device. (b) *I-V* curve of the WSe_2 device in the dark. The device shows linear *I-V* curve in the dark, indicating ohmic contact between the Au electrodes and WSe_2.

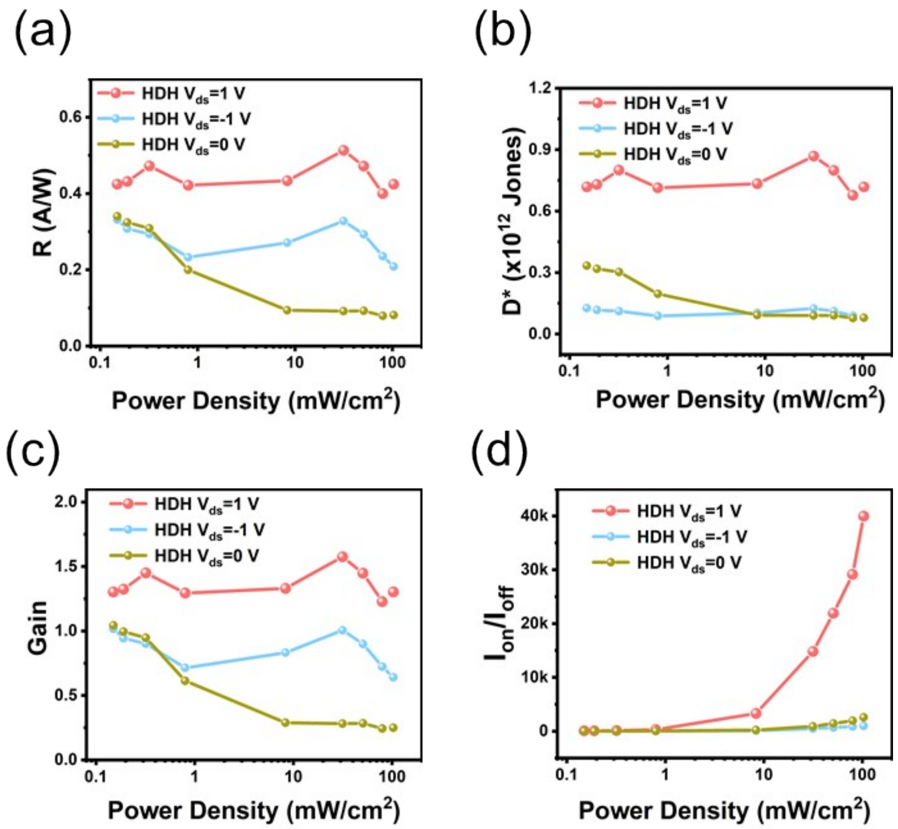

Figure S9. The calculated (a) R, (b) detectivity (D*), (c) Gain, and (d) light on/off ratio (I_{on}/I_{off}) of the HDH device as a function of illumination intensity at the bias of -1 V, 0 V, and 1 V.

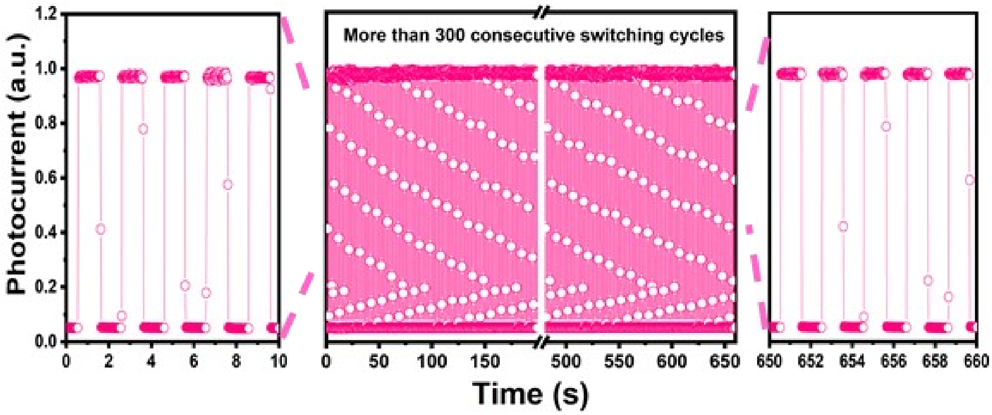

Figure S10. Photoswitching characteristics of the HDH device under pulsed 405 nm light for more than 500 cycles.

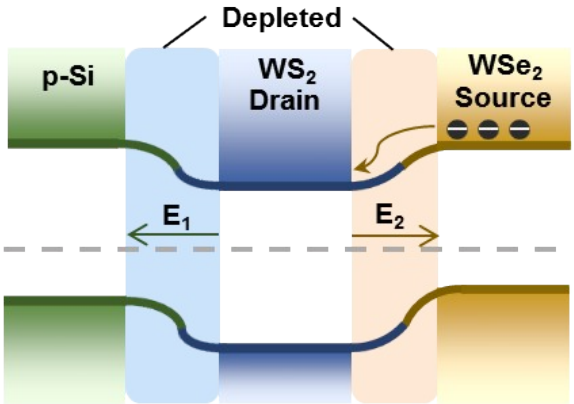

Figure S11. Schematic diagram of the energy band structures of WSe_2/WS_2/p-Si after contact. E_1 and E_2 are the built-in electric fields.

Reference

[1] Zheng, Z.; Yao, J.; Yang, G. Self-Assembly of the Lateral $In_2Se_3/CuInSe_2$ Heterojunction for Enhanced Photodetection. *ACS Appl. Mater. Interfaces* **2017**, *9* (8), 7288-7296.

[2] Chen, K.; Wan, X.; Xie, W.; Wen, J.; Kang, Z.; Zeng, X.; Chen, H.; Xu, J. Lateral

Built-In Potential of Monolayer MoS2-WS2 In-Plane Heterostructures by a Shortcut Growth Strategy. *Adv. Mater.* **2015**, *27* (41), 6431-6437.

[3] Buscema, M.; Island, J. O.; Groenendijk, D. J.; Blanter, S. I.; Steele, G. A.; van der Zant, H. S.; Castellanos-Gomez, A. Photocurrent generation with two-dimensional van der Waals semiconductors. *Chem. Soc. Rev.* **2015**, *44* (11), 3691-3718.

[4] Long, M.; Wang, P.; Fang, H.; Hu, W. Progress, Challenges, and Opportunities for 2D Material Based Photodetectors. *Adv. Funct. Mater.* **2018**, *29* (19),

[5] Yan, F.; Wei, Z.; Wei, X.; Lv, Q.; Zhu, W.; Wang, K. Toward High-Performance Photodetectors Based on 2D Materials: Strategy on Methods. *Small Methods* **2018**, *2* (5),

[6] Gong, C.; Chu, J.; Yin, C.; Yan, C.; Hu, X.; Qian, S.; Hu, Y.; Hu, K.; Huang, J.; Wang, H.; Wang, Y.; Wangyang, P.; Lei, T.; Dai, L.; Wu, C.; Chen, B.; Li, C.; Liao, M.; Zhai, T.; Xiong, J. Self-Confined Growth of Ultrathin 2D Nonlayered Wide-Bandgap Semiconductor CuBr Flakes. *Adv. Mater.* **2019**, *31* (36), 1903580.

[7] Blöchl, P. E. Projector augmented-wave method. *Phys. Rev. B* **1994**, *50* (24), 17953.

[8] Kresse, G.; Joubert, D. From ultrasoft pseudopotentials to the projector augmented-wave method. *Phys. Rev. B* **1999**, *59* (3), 1758.

[9] Kresse, G.; Furthmüller, J. Efficiency of ab-initio total energy calculations for metals and semiconductors using a plane-wave basis set. *Comput. Mater. Sci.* **1996**, *6* (1), 15-50.

[10] Perdew, J. P.; Yue, W. Accurate and simple density functional for the electronic exchange energy: Generalized gradient approximation. *Phys. Rev. B* **1986**, *33* (12), 8800-8802.

[11] Perdew, J. P.; Burke, K.; Ernzerhof, M. Generalized gradient approximation made simple. *Phys. Rev. Lett.* **1996**, *77* (18), 3865.